Research Paper

The Holocene
2024, Vol. 34(8) 1128–1137

DOI: 10.1177/09596836241247311
journals.sagepub.com/home/hol
Sage

Synchronizing the Western Gotland Basin (Baltic Sea) and Lake Kälksjön (central Sweden) sediment records using common cosmogenic radionuclide production variations

Markus Czymzik,[1] Marcus Christl,[2] Olaf Dellwig,[1] Raimund Muscheler,[3] Daniela Müller,[4] Jérôme Kaiser,[1] Markus J Schwab,[5] Carla KM Nantke,[1] Achim Brauer[5,6] and Helge W Arz[1]

Abstract

Multi-archive studies of climate events and archive-specific response times require synchronous time scales. Aligning common variations in the cosmogenic radionuclide production rate via curve fitting methods provides a tool for the continuous synchronization of natural environmental archives down to decadal precision. Based on this approach, we synchronize ^{10}Be records from Western Gotland Basin (WGB, Baltic Sea) and Lake Kälksjön (KKJ, central Sweden) sediments to the ^{14}C production time series from the IntCal20 calibration curve during the Mid-Holocene period ~6400 to 5200 a BP. Before the synchronization, we assess and reduce non-production variability in the ^{10}Be records by using ^{10}Be/^{9}Be ratios and removing common variability with the TOC record from KKJ sediments based on regression analysis. The synchronizations to the IntCal20 ^{14}C production time scale suggest decadal to multi-decadal refinements of the WGB and KKJ chronologies. These refinements reduce the previously centennial chronological uncertainties of both archives to about ± 20 (WGB) and ±40 (KKJ) years. Combining proxy time series from the synchronized archives enables us to interpret a period of ventilation in the deep central Baltic Sea basins from ~6250 to 6000 a BP as possibly caused by inter-annual cooling reducing vertical water temperature gradients allowing deep water formation during exceptionally cold winters.

Keywords

^{10}Be, chronology, Mid-Holocene climate, sediment archives, time scale synchronization, western Baltic region

Received 22 January 2024; revised manuscript accepted 29 February 2024

Introduction

Paleoclimate reconstructions provide insights into past climate dynamics and, thereby, improve our understanding of the climate system (Rasmussen et al., 2014; von Grafenstein et al., 1999). Multi-archive investigations of these reconstructions allow us to study leads and lags in proxy responses to climate changes providing information about their temporal progression and spatial gradients, archive-specific thresholds and the driving mechanisms (Czymzik et al., 2020; Fleitmann et al., 2009). However, due to the often considerable uncertainties of the archives' individual chronologies, such detailed studies require independent synchronization tools.

For sedimentary archives, volcanic ash (tephra) deposits provide such a tool (Blockley et al., 2014; Wulf et al., 2013). The geochemical fingerprint of tephra deposits provides stratigraphic isochrones enabling the alignment of different sediment archives (Lane et al., 2015). However, this method is limited by the stochastic occurrence of large volcanic eruptions and regionally restricted fallout patterns. Matching globally common production rate variations of cosmogenic radionuclides using curve fitting methods can provide a continuous synchronization tool for environmental archives (Czymzik et al., 2016; Mellström et al., 2015; Muscheler et al., 2014; Snowball et al., 2010).

Cosmogenic radionuclides like ^{10}Be and ^{14}C are produced in Earth's upper atmosphere by the interaction of atmospheric target nuclei with incident galactic cosmic rays (Lal and Peters, 1967). Varying helio- and geomagnetic shielding of these galactic cosmic rays result in a characteristic cosmogenic radionuclide production and fallout pattern imprinted in environmental

[1]Leibniz Institute for Baltic Sea Research Warnemünde (IOW), Marine Geology, Germany
[2]ETH Zurich, Laboratory of Ion Beam Physics, Switzerland
[3]Quaternary Sciences, Lund University, Sweden
[4]Institute of Earth Sciences, Heidelberg University, Germany
[5]Climate Dynamics and Landscape Evolution, GFZ German Research Centre for Geosciences, Germany
[6]Institute of Geosciences, University of Potsdam, Germany

Corresponding author:
Markus Czymzik, Leibniz Institute for Baltic Sea Research Warnemünde (IOW), Marine Geology, Seestraße 15, Rostock 18119, Germany.
Email: markus.czymzik@io-warnemuende.de

archives around the globe (Aldahan and Possnert, 1998; Lal and Peters, 1967; Simon et al., 2020). Placing sedimentary ^{10}Be records on the precise ^{14}C production rate time scale from the IntCal20 calibration curve using curve fitting methods enables us to synchronize these records and reduce the uncertainties of the connected chronologies (Czymzik et al., 2018, 2020).

A challenge of this method is the unequivocal detection of the ^{10}Be production signal due to postproduction influences mainly introduced by the redeposition of previously deposited "old" ^{10}Be, varying atmospheric circulation and sedimentology (Balco et al., 2021; Czymzik et al., 2015; Simon et al., 2016). One way to reduce these influences is the analysis of ^{10}Be/^{9}Be-ratios (Wittmann et al., 2012). Introduced into a natural environment ^{10}Be and ^{9}Be behave chemically identical. However, while ^{10}Be is produced in the atmosphere, ^{9}Be originates from weathering crustal rocks (Simon et al., 2020; Wittmann et al., 2012). Therefore, common variations of both isotopes in a sediment archive can be assumed to mainly reflect transport of previously deposited "old" ^{10}Be and ^{9}Be within the lake/catchment setting and the ^{10}Be/^{9}Be-ratio an environment-corrected record of the atmospheric ^{10}Be production rate (Savranskaia et al., 2021). Another correction method comprises regression analyses between ^{10}Be records and environmental proxy time series from the same sediment core (Czymzik et al., 2018). Thereby, it is assumed that common variability with a proxy record represents an environmental bias in the ^{10}Be record. However, due to the sole statistical nature, the results of this approach require a discussion about the underlying mechanisms.

Previous studies on the Lake Kälksjön (KKJ, central Sweden) sediment sequence successfully applied ^{14}C wiggle-match dating to connect its chronology to the IntCal time scale around ~8200 and between 3000 and 2000 a BP, with errors of down to ±20 years (Mellström et al., 2015; Snowball et al., 2010). In the following, we attempt to synchronize ^{10}Be records from brackish Western Gotland Basin (WGB, Baltic Sea) and terrestrial KKJ sediments to the ^{14}C production time-series inferred from the IntCal20 calibration curve during the Mid-Holocene period ~5200 to 6400 a BP. Favorable for the synchronization, this period includes a succession of distinct centennial cosmogenic radionuclide production peaks. Considering the high replication of the underlying ^{14}C data and dendrochronological precision of this part of the calibration curve, we use it as an absolute dated target time series (Reimer et al., 2020). Before the synchronization, the ^{10}Be data from WGB and KKJ sediments were corrected for the average atmospheric residence time of ~1 year (Raisbeck et al., 1981) and possible non-production influences. Based on the synchronized records, we investigate the likely driving mechanisms of a period of ventilation and deposition of well-mixed sediments in the central Baltic Sea basins ~6250 to 6000 a BP (Moros et al., 2020; Warden et al., 2017).

Study sites

The presently brackish Baltic Sea formed ~8000 years ago mainly as a result of post-glacial sea-level rise (Figure 1) (Björck, 1995). Competing inflows of saline waters from the North Sea via the shallow Danish Straits and freshwater from rivers and precipitation led to the establishment of a strong pycnocline (Emeis et al., 2003). Its morphologically complex basin is subdivided through sills and connected by channels (Leppäranta and Myrberg, 2009). Postglacial isostatic land uplift successively modifies water depths and shoreline positions (Berglund et al., 2005; Ekman, 1996). Continuous sediment accumulation is restricted to the deeper areas of the Baltic Sea, while wave-induced sediment transport or erosion becomes dominant in shallower and coastal regions (Winterhalter, 1992). Only within the deep basins finely laminated organic-rich sediments can deposit under predominantly oxygen-deficient and sulfidic bottom water conditions (Andrén et al., 2000; Zillén et al., 2008). An exception is the modern period where the effects of anthropogenic forcing and global warming favored anoxia and the deposition of fine laminated sediments also in some shallow coastal basins (Jokinen et al., 2018). The Baltic Sea has a surface area of 377,000 km^2 and catchment size of 1,641,650 km^2. Its mean depth is 54 m and the deepest point is located in the funnel-shaped Landsort Deep (459 m) (BACC, 2015). The WGB is located in the central Baltic Sea, off south-eastern Sweden (Figure 1).

KKJ is situated in central Sweden (60°09′N/13°02′E; 97 m a.s.l.), ~250 km west of the Baltic Sea coast (Figure 1). KKJ was isolated from ancient Lake Vänern ~9600 years ago through isostatic uplift (Czymzik et al., 2023; Mellström et al., 2015; Stanton et al., 2010). The present basin has a catchment size of 4 km^2, surface area of 0.42 km^2 and maximum water depth of 13.6 m. Four minor creeks discharge into KKJ from the forested northern and eastern catchment (Stanton et al., 2010). The lake's only outflow in the West was artificially incised in 1878 CE (Czymzik et al., 2023).

Material and methods

Sediment cores and initial chronologies

Sediment core M86-1a/33-4GC (58°21.9N/17°50.0E) was retrieved from the WGB at 101 m water depth using a gravity corer during a cruise with RV Meteor in 2011 (Figure 1). Age constraints for the investigated sediment interval from 189 to 219 cm core depth were transferred from the radiometrically dated Eastern Gotland Basin sediment core P435-2-1, through matching common variability in the loss-on-ignition (LOI) and XRF Br organic matter proxies (Warden et al., 2017).

Sediment core KKJ19 was retrieved from the central basin of the lake in 2019 using an UWITEC piston corer (Czymzik et al., 2023). The age-depth model for sediment core KKJ19 was built using 8 calibrated AMS ^{14}C ages, ^{137}Cs and ^{241}Am measurements, as well as lithological marker layers of known age (Czymzik et al., 2023).

Beryllium extraction and measurements

For the extraction and measurement of ^{10}Be and ^{9}Be records at ~20 to 30-year resolution, series of samples were collected at 0.5 cm step-size from sediment core M86-1a/33-4GC and 1 cm resolution from sediment core KKJ19. After spiking with 0.2 mg ^{9}Be carrier, Be was leached from 0.2 g freeze-dried and homogenized sediment samples overnight with 32 vol% HCl and H_2O_2 (Henken-Mellies et al., 1990). The resulting solution was separated from the remaining material through centrifuging. Then, hydroxides were precipitated at pH 10 using 25 vol% NH_4OH and separated from the solution by centrifuging. Be was co-precipitated with Fe using 25 vol% NH_4OH and then re-dissolved by increasing the pH to 14 with NaOH. $Be(OH)_2$ was precipitated from the remaining solution using 25 vol% NH_4OH at pH 8–10 and washed two times with ultra-pure H_2O. After oxidizing at 600°C in a muffle furnace, BeO was mixed with Nb and pressed into cathodes for AMS measurements. Final ^{10}Be concentrations were calculated from measured ^{10}Be/^{9}Be ratios, normalized to the S2007N (^{10}Be/^{9}Be = 28.1×10^{-12}) and S2010N (^{10}Be/^{9}Be = 3.3×10^{-12}) reference standards (Christl et al., 2013).

^{9}Be was extracted from aliquots of the same sediment samples as for ^{10}Be. The procedure includes treatment with 15 vol% HCl for 1 h on a shaker, centrifuging, decanting and cleaning through a 0.4 µm mesh-size filter. Measurements of ^{9}Be contents were conducted with a quadrupole ICP-MS (iCAP Q, Thermo Fisher Scientific) using matrix-matched external calibration. Rhodium served as internal standard to compensate for instrument fluctuations and remaining matrix effects. Precision and accuracy were

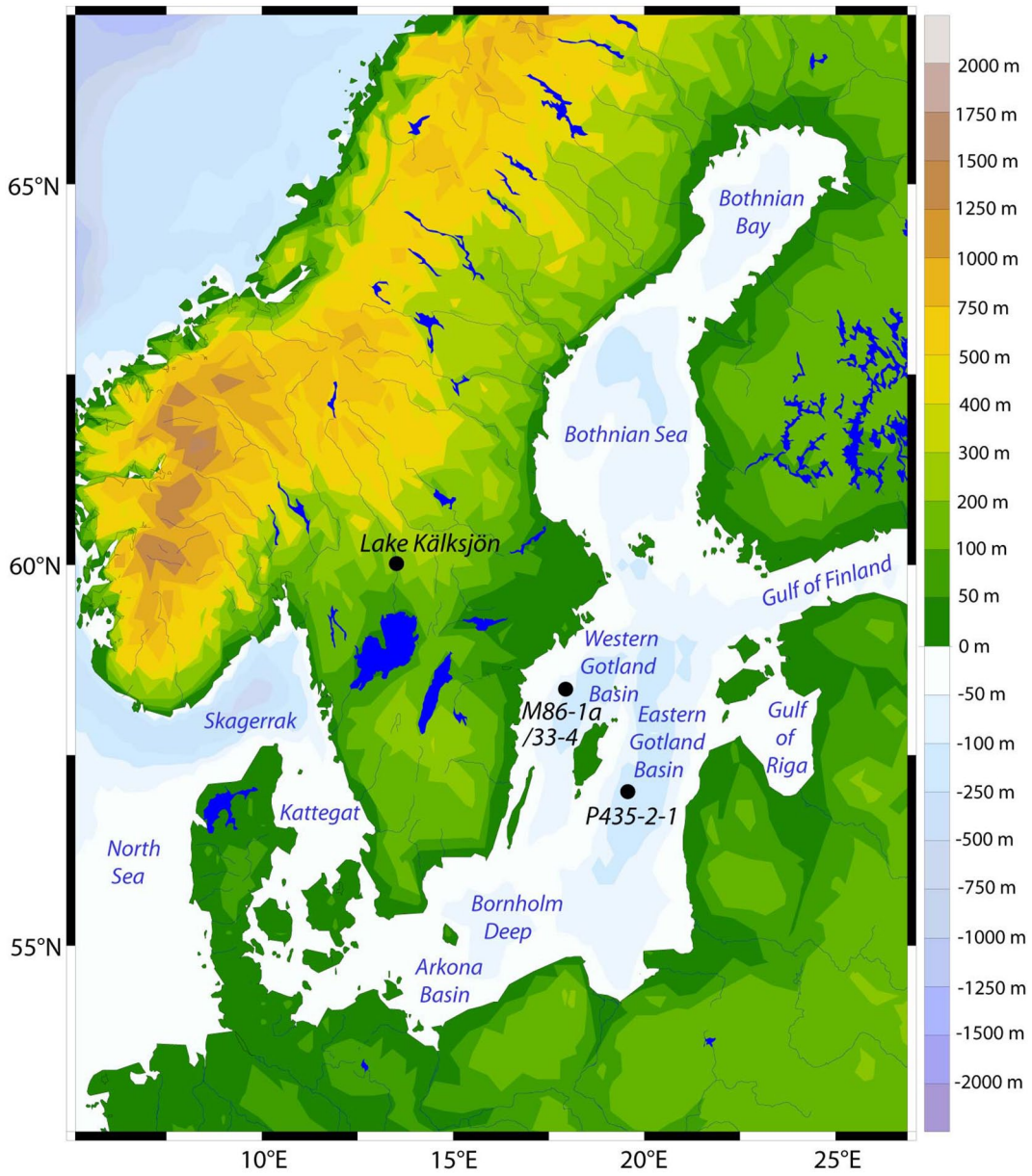

Figure 1. Geographical locations of sediment cores M86-1a/33-4GC from the Western Gotland Basin (WGB) and P435-2-1 from the Eastern Gotland Basin, as well as Lake Kälksjön (KKJ) in central Sweden. Map modified after Kaiser et al. (2017).

checked by the international sediment reference materials SGR-1b (USGS) and TH-2 (Canada) and were better than 1.6% and 3.9%, respectively. Because no certified Be contents were available for the here-applied HCl extraction, both materials were subjected to total acid digestion using a HNO_3–HF–$HClO_4$-mixture, to determine the analytical error (Dellwig et al., 2019).

XRF element profiles and loss on ignition

X-ray fluorescence (XRF) measurements at 200 µm resolution were conducted on WGB sediment core M86-1a/33-4GC using an ITRAX core scanner with a Cr tube and an energy-dispersive SDD detector (Croudace et al., 2019). The 10 mm wide X-ray beam was orientated parallel to the laminations, to minimize the effects of sediment micro-disturbances. Individual measurements were performed at 30 kV and 30 µA, with a dwell time of 15 s. Loss on ignition (LOI) was determined at 1 cm resolution from freeze-dried samples of sediment core M86-1a/33-4GC, combusted for 3 h at 550°C. Sediment core M86-1a/33-4GC includes no considerable amounts of diagenetic Mn carbonate that would bias organic matter estimates from LOI data (Häusler et al., 2017).

Correcting for environmental influences on ^{10}Be concentrations

To detect and correct for non-production-related biases in the ^{10}Be records from WGB and KKJ sediment cores, two approaches were applied. First, we use ratios of the isotopes ^{10}Be (meteoric production and redeposition) and ^{9}Be (released from weathering rocks and redeposition) to remove environmental biases from our ^{10}Be concentration records (Simon et al., 2020; Wittmann et al., 2012). Second, we compare the ^{10}Be concentration records with proxy time series from the same archives, reflecting the main sediment constituents (organic matter: WGB = LOI, KKJ = TOC (Czymzik et al., 2023); detrital material: WGB = Ti/Br, KKJ = Ti (Czymzik et al., 2023). Ti/Br can be used to reduce the effects of varying organic matter contents on XRF Ti counts in marine sediments (Ziegler et al., 2008). In case of a significant correlation, we removed the covariance from the ^{10}Be concentration record

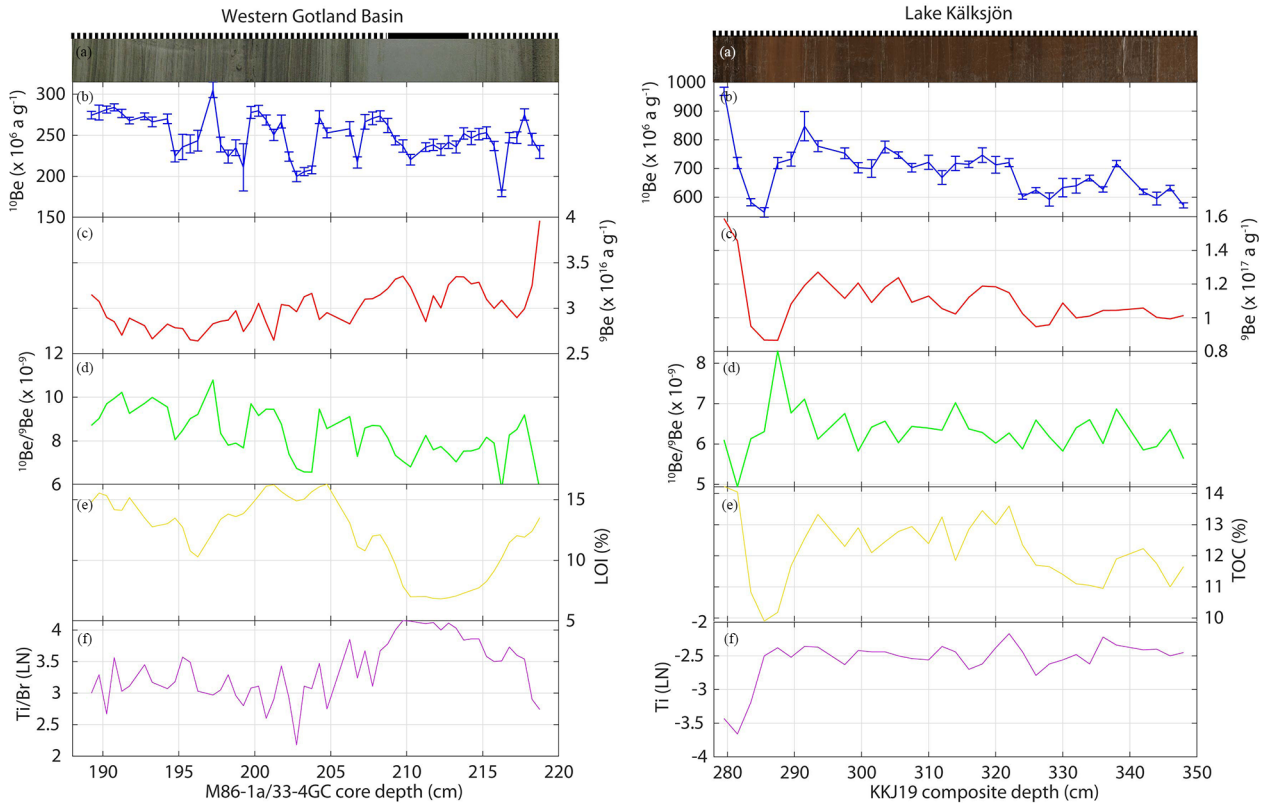

Figure 2. Investigated parts of Western Gotland Basin (WGB) and Lake Kälksjön (KKJ) sediment cores with Be and selected proxy data. (a) Photographs of the investigated parts of sediment cores M86-1a/33-4GC (intervals with laminated and homogeneous sediments are indicated) and KKJ19, (b) ^{10}Be, (c) ^{9}Be, (d) ^{10}Be/^{9}Be, (e) organic matter proxies (WGB: LOI, KKJ: TOC), (f) detrital matter proxies (WGB: Ti/Br, KKJ: Ti).

using linear regression (only TOC in KKJ=^{10}Be$_{TOC}$) (Adolphi and Muscheler, 2016; Czymzik et al., 2020).

^{14}C production rates

^{14}C production rates used in this study were calculated using a box-diffusion carbon cycle model assuming no changes in the global carbon cycle over the investigated period (Muscheler et al., 2005; Siegenthaler, 1983). The uncertainties of the IntCal20 calibration curve were included by using 100 posterior realizations of possible atmospheric ^{14}C curves, obtained by fitting Bayesian splines to the ^{14}C data underlying IntCal20 (Heaton et al., 2020; Reimer et al., 2020). The reported ^{14}C production rate reflects the average obtained from the 100 realizations.

Time scale synchronization and propagating uncertainties

The ^{10}Be/^{9}Be-ratio time series from both archives, as well as the TOC-corrected ^{10}Be record from KKJ sediments were semi-automatically synchronized to the atmospheric ^{14}C production record from the IntCal20 calibration curve using the MATCH software working with the global optimal fit (Lisiecki and Lisiecki, 2002; Reimer et al., 2020). MATCH divides the records into small segments and calculates all possible alignments to find the optimal one. The alignment score is expressed as the square of the difference between the two signals (Lisiecki and Lisiecki, 2002). Before the synchronization, all data were detrended and z-score transformed by subtracting the mean and dividing by the standard deviation (Lisiecki and Lisiecki, 2002). Up to ±25% changes in sedimentation rates were allowed to account for the effects of chronological and sampling uncertainties and all realizations with at least 1-year difference included in the calculation of the final mean synchronization results. Error margins for the synchronization procedure were determined by applying root mean squared error (RMSE) estimates, considering two identified uncertainties and using the following formula (Grant et al., 2012):

$$\mathrm{RMSE} = \sqrt{\left(a^2 + b^2\right)}$$

(a) Synchronization uncertainty, defined as the maximum difference between the individual synchronization realizations.
(b) Sample resolution of the ^{10}Be records.

Results

Beryllium inventories and sediment composition

Concentrations of ^{10}Be and ^{9}Be were measured in 54 samples from WGB sediments covering the interval from 189 to 219 cm core depth. ^{10}Be concentrations vary between 179.4 and 305.3 × 10^6 a g^{-1}, around a mean of 248.7 × 10^6 a g^{-1} (Figure 2). The ^{10}Be record from WGB sediments shows cm-scale excursions and amplitude changes of ~50% throughout the record (Figure 2). One ^{10}Be data point from an earlier series was excluded from the analyses, due to uncertainties regarding the added ^{9}Be tracer. Correlations of ^{10}Be in WGB sediments with the organic (LOI: r=0.04, p=0.41) and detrital matter (Ti/Br: r=0.15, p=0.12) proxies are very low (Figure 3). ^{9}Be contents in WGB sediments range from 2.6 to 4 × 10^{16} a g^{-1} (mean 3 × 10^{16} a g^{-1}) and show a slightly increasing trend between 189 and 217 cm core depth (Figure 2).

^{10}Be and ^{9}Be concentrations were measured in 33 samples from KKJ sediments. ^{10}Be concentrations range from 547.1 to 968.8 × 10^6 a g^{-1}, around a mean of 690.7 × 10^6 a g^{-1} (Figure 2). The ^{10}Be record reveals smaller variations between 290 and

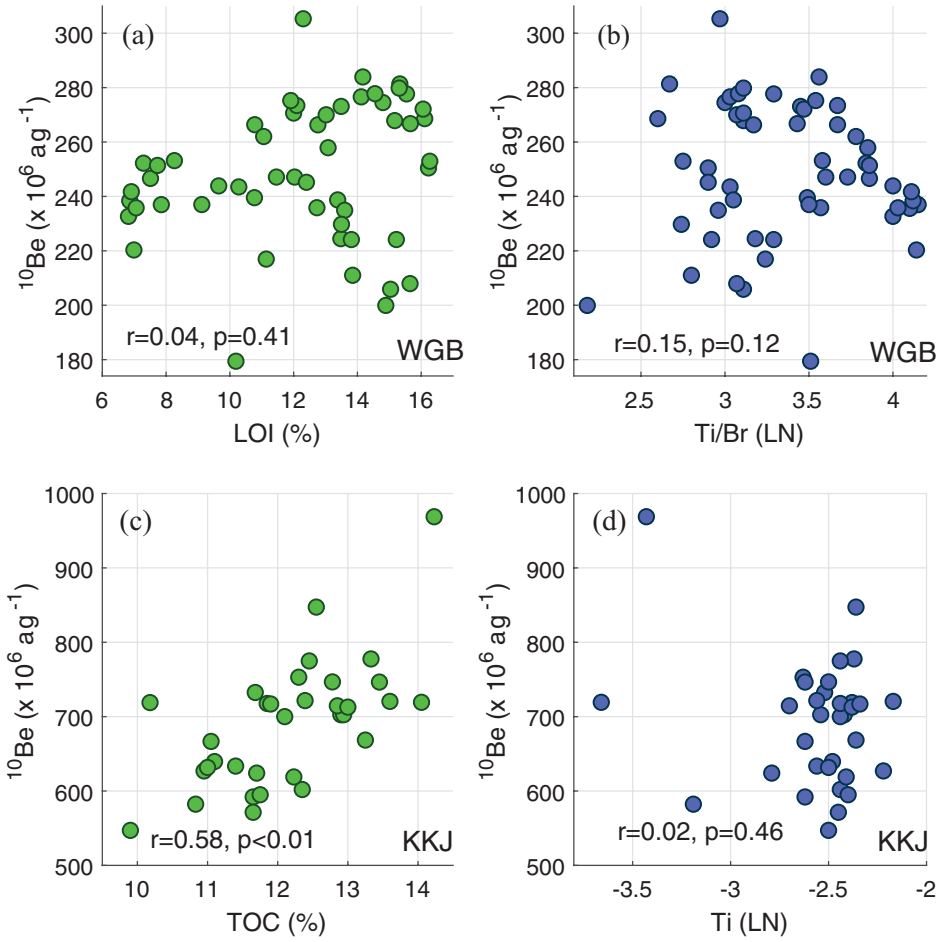

Figure 3. Correlations of ^{10}Be records from Western Gotland Basin (WGB) and Lake Kälksjön (KKJ) sediments with proxy records of changing organic and detrital matter contents. (a) Organic matter proxy loss on ignition (LOI) and ^{10}Be in WGB sediments. (b) Detrital matter proxy Ti/Br and ^{10}Be in WGB sediments. (c) Organic matter proxy total organic carbon (TOC) and ^{10}Be in KKJ sediments. (d) Detrital matter proxy Ti and ^{10}Be in KKJ sediments.

350 cm core depth and a larger excursion from 280 to 290 cm core depth (Figure 2). ^{10}Be concentrations from KKJ sediments reveal a significant correlation with the TOC record from this archive ($r = 0.58$, $p < 0.01$) (Figure 3). The correlation between ^{10}Be and the detrital matter proxy Ti in KKJ sediments is very low ($r = 0.02$, $p = 0.46$) (Figure 3). ^{9}Be concentrations in KKJ sediments reach from 0.87 to 1.59×10^{17} a g^{-1} (mean 1.1×10^{17} a g^{-1}) (Figure 2). Blank corrections were negligible for the ^{10}Be data from WGB and KKJ sediments.

Discussion

Mechanisms of ^{10}Be deposition in WGB and KKJ sediments

Changing sediment composition and the redeposition of "old" ^{10}Be can bias the expected ^{10}Be production signal in sediment records (Berggren et al., 2010; Czymzik et al., 2018). This chapter aims at disentangling the mechanisms of ^{10}Be deposition in WGB and KKJ sediments.

Very low correlations with ^{9}Be, the organic and detrital matter proxies, as well as resemblances with the ^{10}Be/^{9}Be and ^{14}C production records indicate minor environmental influences and a good preservation of the ^{10}Be production rate variations in WGB sediments (Figures 2–5). Amplitude changes of ~60% for most of the record match the expected production rate variations during centennial-scale solar variability changes (Muscheler and Heikkilä, 2011) (Figure 4).

Two exceptions are the short sediment intervals around 192 cm and from 210 to 214 cm core depth (Figure 2). Between 210 and 214 cm core depth (~6300 to 6100 a BP), no decadal-scale variability is preserved in the ^{10}Be and ^{10}Be/^{9}Be records from WGB sediments, in contrast to the ^{14}C production time-series (Figures 2 and 5). This interval corresponds broadly to a non-laminated sediment unit in the WGB sediment core that is a common stratigraphic feature in the deep central Baltic Sea basins (Warden et al., 2017; Zillén et al., 2008). It is interpreted to be mainly triggered by water turbulences during ventilation causing sediment redeposition and mixing (Moros et al., 2020; Warden et al., 2017). Assumedly, sediment mixing also led to a smoothing the ^{10}Be and ^{10}Be/^{9}Be records from WGB sediments during this interval.

In turn, a minimum in the ^{14}C production record without a corresponding response in the WGB ^{10}Be record around 192 cm core depth (~5300 a BP) can be corrected for using ^{10}Be/^{9}Be-ratios (Figures 4 and 5). Therefore, the main reason likely is an enhanced contribution of "old" ^{10}Be to the coring site that is paralleled by a similar enrichment of ^{9}Be, without substantial sediment mixing at the coring site (Figure 5).

In contrast to ^{10}Be in WGB sediments (except for 192 cm core depth), ^{10}Be concentrations in KKJ sediments reveal significant correlations ($p < 0.01$) with the ^{9}Be and TOC records from this archive (Figure 3). These correlations point to a strong environmental influence on ^{10}Be deposition in the lake. TOC contents in KKJ sediments during the last ~9600 years were interpreted to predominantly reflect productivity changes controlled by North Atlantic Oscillation (NAO) driven winter temperature influences

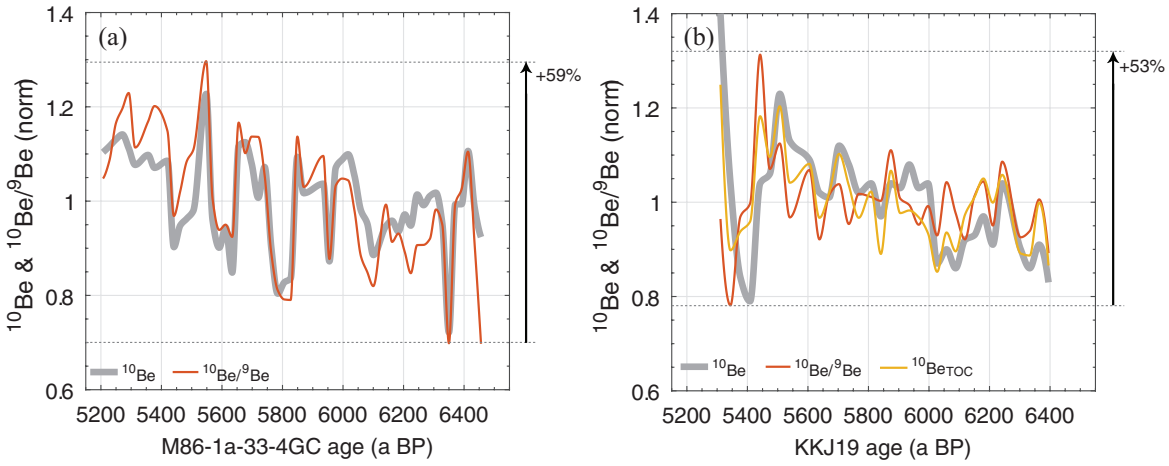

Figure 4. Correcting for environmental influences on ^{10}Be deposition in (a) Western Gotland Basin (WGB) and (b) Lake Kälksjön (KKJ) sediments using ^{10}Be/^{9}Be-ratios and regression analysis with the significantly correlated TOC record from KKJ sediments.

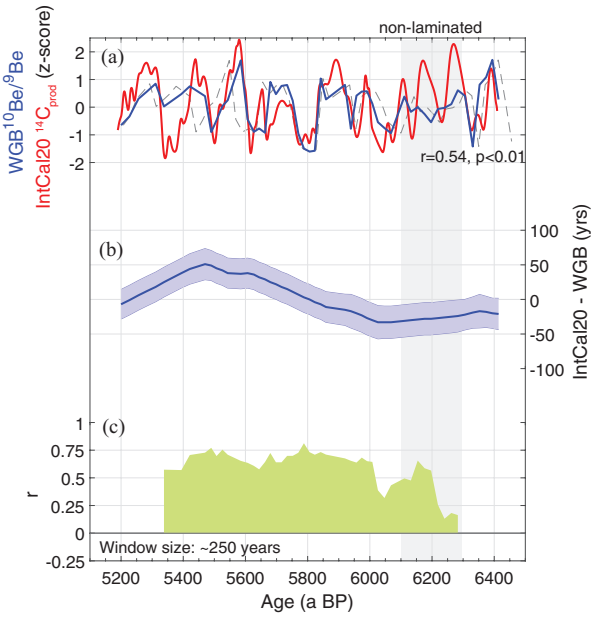

Figure 5. Synchronization of ^{10}Be/^{9}Be record from Western Gotland Basin (WGB) sediments with ^{14}C production rates from the IntCal20 calibration curve (Reimer et al., 2020). (a) ^{10}Be/^{9}Be record (blue) synchronized to ^{14}C production rates (red). The dashed line depicts the ^{10}Be/^{9}Be record on its original time scale. The significance of the correlation coefficient takes into account the effects of autocorrelation in the time series (Ebisuzaki, 1997). (b) Chronological changes applied to the ^{10}Be/^{9}Be record during the synchronization with root mean square error (RMSE) estimates (Grant et al., 2012). (c) Moving correlation between the synchronized ^{10}Be/^{9}Be and ^{14}C production records.
Note. Please refer to the online version of the article to view this figure in color.

on ice cover duration and growth season length (for a detailed discussion see Czymzik et al., 2023). Sedimentary TOC contents are enhanced when the ice cover duration is shortened and the growing season prolonged (Czymzik et al., 2023). In consequence, a prolonged (shortened) ice cover season might also restrict (increase) ^{10}Be and ^{9}Be transport from the catchment into KKJ. In addition, most of the ^{10}Be record from KKJ sediment reveals amplitude variations of only ~20–30% (Figure 4). These variations do not match the expected ~50% ^{10}Be production rate changes connected with centennial-scale solar variability (Muscheler and Heikkilä, 2011).

Nevertheless, covariance between the ^{14}C production time series, as well as ^{10}Be/^{9}Be and TOC corrected ^{10}Be records from KKJ sediments for most of the investigated time-span point to a removal of the main environmental bias (Figure 6). Some remaining inconsistencies might point to further unresolved environmental influences and advise against the interpretation of small-scale features in terms of cosmogenic radionuclide production rate changes (Muscheler et al., 2014) (Figure 6).

Synchronizing the WGB and KKJ sediment records to the IntCal20 ^{14}C time-scale

Shared variability in ^{10}Be and ^{14}C records can be interpreted in terms of common changes in cosmogenic radionuclide production and serves as a tool for the synchronization of different environmental archives based on curve fitting (Czymzik et al., 2020; Mekhaldi et al., 2020; Mellström et al., 2015; Snowball et al., 2010). Semi-automatic alignment using the best fit was applied to synchronize the environment-corrected ^{10}Be records from WGB (^{10}Be/^{9}Be) and KKJ (^{10}Be/^{9}Be and ^{10}Be$_{TOC}$) sediments to the ^{14}C production time series from the IntCal20 calibration curve (Figures 5 and 6).

The synchronized ^{10}Be/^{9}Be record from WGB sediments reveals a significant positive correlation with the ^{14}C production time series ($r = 0.54$, $p < 0.01$) (Figure 5). Moving correlations with a window-size of 250 years indicate correlation coefficients between 0.57 and 0.81 from 5200 to 6000 a BP and, as expected, reduced correlations between 0.13 and 0.66 for the part of the WGB ^{10}Be/^{9}Be record from non-laminated sediments with a smoothed ^{10}Be production signal (Figure 5). Compared to the ^{14}C production time-series from IntCal20, the WGB ^{10}Be/^{9}Be record before the synchronization appears up to 51 years younger between 5300 and 5700 a BP and up to 33 years older from 6000 to 6200 a BP (Figure 5). The applied chronological changes are outside the ±21–24 years RMSE uncertainties for the synchronization procedure for most of the record, but within the centennial chronological uncertainties of the ^{14}C dated WGB record (Figure 5) (Warden et al., 2017).

The synchronized ^{10}Be/^{9}Be and ^{10}Be$_{TOC}$ records from KKJ sediments reveal significant positive correlations with the ^{14}C production time series (Figure 6). Moving correlations vary between 0.39 and 0.94 for the ^{10}Be/^{9}Be-ratio, as well as 0.4 and 0.87 for the ^{10}Be$_{TOC}$ record. Exceptions are short intervals with correlation coefficients down to <0.2 at ~6050 and 5700 a BP for the ^{10}Be/^{9}Be, as well as ~5800 a BP for the ^{10}Be$_{TOC}$ record corresponding to short-term mismatches possibly associated with secondary ^{14}C peaks that are not resolved in the KKJ ^{10}Be record at ~30-year resolution (Figure 6).

The chronological refinements suggested by the applied synchronizations for KKJ sediments are similar for both the

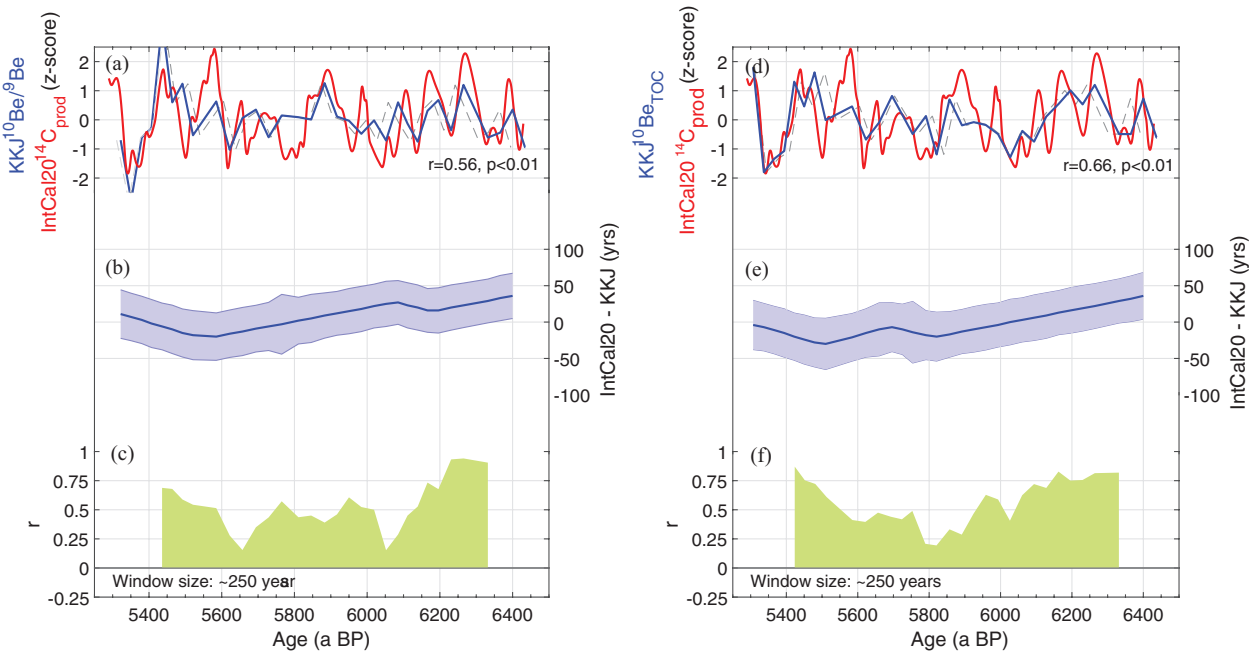

Figure 6. Synchronization of $^{10}Be/^{9}Be$ and TOC corrected ^{10}Be records from Lake Kälksjön (KKJ) sediments with ^{14}C production rates from the IntCal20 calibration curve (Reimer et al., 2020). (a) $^{10}Be/^{9}Be$ record (blue) synchronized to ^{14}C production rates (red). The dashed line depicts the $^{10}Be/^{9}Be$ record on its original time-scale. The significance of the correlation coefficient takes into account the effects of autocorrelation in the time-series (Ebisuzaki, 1997). (b) Chronological changes applied to the $^{10}Be/^{9}Be$ record during the synchronization with root mean square error (RMSE) estimates (Grant et al., 2012). (c) Moving correlation between the synchronized $^{10}Be/^{9}Be$ and ^{14}C production records. (d) Same as (a), but for the TOC corrected ^{10}Be record from KKJ sediments. (e) Same as (b), but for the TOC corrected ^{10}Be record from KKJ sediments. (f) Same as (c), but for the TOC corrected ^{10}Be record from KKJ sediments.
Note. Please refer to the online version of the article to view this figure in color.

$^{10}Be/^{9}Be$-ratio and $^{10}Be_{TOC}$ records (Figure 6). They suggest that the KKJ chronology is about 20 years too old between 5300 and 6000 a BP and 40 years too young in the interval from 6200 to 6400 a BP (Figure 6). All performed chronological changes occur within the RMSE uncertainties of the applied synchronization procedure ($^{10}Be/^{9}Be$: ±30-41 years; $^{10}Be_{TOC}$: ±30-42 years) and ^{14}C-based chronology of the KKJ sediment core (Czymzik et al., 2023). The resulting uncertainty ranges for the here applied synchronization procedure are slightly larger than the ±20 years from ^{14}C wiggle-match dating of KKJ sediments from 3000 to 2000 a BP, likely due to our continuous sampling strategy that was not adjusted to changes in the ^{14}C calibration curve (Mellström et al., 2015).

Baltic Sea ventilation ~6250 to 6000 a BP

Oxygen levels and sediment deposition in the deep basins of the central Baltic Sea before the time of major human interferences were predominantly modulated by coinciding centennial climate periods (Andrén et al., 2000; Moros et al., 2020; Zillén et al., 2008). Warmer periods like the Holocene Thermal Maximum (HTM; ~8000 to 5000 a BP), Roman Period (~2200 to 1500 a BP) and Medieval Climate Anomaly (~1300 to 800 a BP) were accompanied by strengthened water column stratification and the preservation of finely laminated sediments under anoxic conditions (Moros et al., 2020; Wanner et al., 2011). Colder periods during the Neoglaciation (~4000 to 2200 a BP) and Little Ice Age (~500 to 100 a BP) are paralleled by water column ventilation and lateral sediment transport causing the deposition of homogenous sediments in the deep Baltic Sea basins (Moros et al., 2020; Zillén et al., 2008). A proposed mechanism is deep water formation during colder winters (Moros et al., 2020). One seemingly exception to this general pattern is a period of homogenous sedimentation in the central Baltic Sea basins between ~6250 and 6000 a BP, intercalated into the finely laminated sediments of the HTM (Warden et al., 2017) (Figure 7). This period is broadly coincident with a shorter cold period predominantly in the southern Hemisphere, North America and Greenland (Lecavalier et al., 2017; Wanner et al., 2011) and intercalated into intervals of distinct stratification in the Bothnian Sea (Kaiser et al., 2024).

Comparing the occurrence of this homogenous sediment sequence with temperature proxies from the synchronized Baltic Sea and KKJ sediments covering most of the HTM, allows us to investigate the possible triggering mechanisms, with high chronological accuracy. Before the comparison, the here applied chronological refinements of WGB sediment core M86-1a/33-4GC were transferred to Eastern Gotland Basin sediment core P435-2-1 providing a TEX_{86} biomarker record (Warden et al., 2017; Wittenborn et al., 2022). Downcore calibration studies indicate this record to reflect central Baltic Sea water temperatures at 80–120 m depth, controlled by inter-annual to decadal changes in regional air temperature (Meier, 2005; Wittenborn et al., 2022).

The interval of homogenous sedimentation is paralleled by reduced inter-annual air temperatures in the central Baltic Sea region, reflected by the TEX_{86} record (Figure 7) (Wittenborn et al., 2022). Moreover, this interval coincides with colder winters, imprinted in reduced TOC contents of KKJ sediments (Czymzik et al., 2023). Periods of reduced TOC contents in KKJ sediments were interpreted to reflect colder winters reducing growth season length during a prevailing negative mode of the North Atlantic Oscillation (NAO) (for details see Czymzik et al., 2023). Its association with changes in NAO polarity supports a central Baltic Sea basin wide geographic relevance of the recorded TOC signal in KKJ sediments (Czymzik et al., 2023). However, cooler temperatures during this period were not unique and comparably cold intervals occurred from 6800 to 6500 a BP in the Baltic Sea record, and around 5400 and 6450 a BP in the KKJ data (Figure 7).

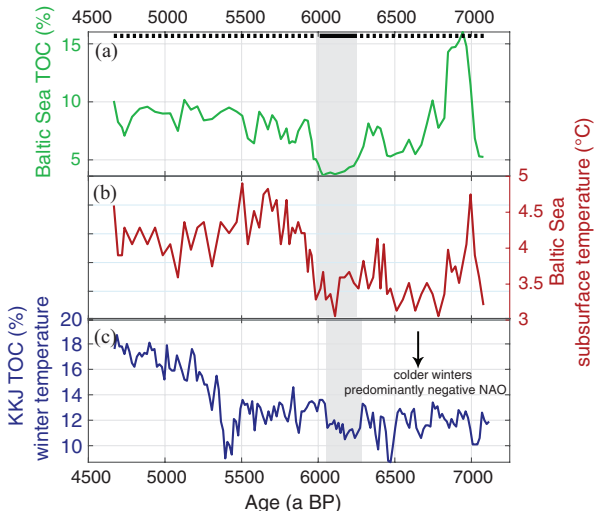

Figure 7. Comparison of synchronized paleoenvironmental records from Baltic Sea and Lake Kälksjön (KKJ) sediments. (a) Total organic carbon (TOC) record from Baltic Sea sediment core P435-2-1 (Warden et al., 2017). (b) TEX_{86} record from Baltic Sea sediment core P435-2-1 interpreted to reflected subsurface water temperatures at 80–120 m depth (Warden et al., 2017; Wittenborn et al., 2022). (c) TOC record from Lake Kälksjön (KKJ) sediments interpreted to reflect North Atlantic Oscillation (NAO) driven changes in ice cover and winter temperatures (Czymzik et al., 2023). All records were synchronized to the IntCal20 ^{14}C time scale based on the existing ^{10}Be data from both archives (~6400-5200 a BP). Within the older and younger parts bracketing this interval, age offsets from the start and end-points of the synchronization were extrapolated. The gray bar highlights the discussed cold reversal within the HTM resulting in homogenous sediments deposition in the central Baltic Sea basins.

The perhaps exceptional feature during the period of homogenous sediment deposition from 6250 to 6000 a BP is the coinciding decrease in both, inter-annual (Baltic Sea) and winter (KKJ) temperatures (Figure 7). Therefore, we speculate that such inter-annual cooling might have been prerequisite to sufficiently reduce vertical water temperature gradients and allow deep water formation in the central Baltic Sea basins during exceptionally cold winters, also within the generally warmer HTM conditions (Moros et al., 2020). The slight temporal lag of the central Baltic Sea TEX_{86} temperature record compared to the winter temperature time series from KKJ sediments might reflect a delay of ~10 years required for the atmospheric temperature signal to propagate into the deeper Baltic Sea water column, where it is transferred into the biomarker temperature proxy by biosynthesizing archaea (Figure 7) (Meier, 2005; Wittenborn et al., 2022).

Conclusions

We present two new ^{10}Be records from brackish WGB and lacustrine KKJ sediments covering the time interval from ~6400 to 5200 a BP. $^{10}Be/^{9}Be$-ratios from both archives, as well as regression analysis with the correlating TOC record from KKJ sediments, reduced non-production signals in the measured ^{10}Be records.

Significant correlations between the ^{10}Be and $^{10}Be/^{9}Be$ records from WGB sediments with the ^{14}C production rate time series from the IntCal20 calibration curve indicate that environmental influences on ^{10}Be concentrations in the investigated sediment section are minor. The main exception is a ~4 cm thick non-laminated sediment unit without decadal-scale ^{10}Be production variations, likely smoothed out by turbulent sediment mixing. Similarities between the ^{10}Be, ^{9}Be and TOC records from KKJ sediments, in turn, point to a climate influence on ^{10}Be deposition in this archive. However, significant correlations of the $^{10}Be/^{9}Be$ and $^{10}Be_{TOC}$ records with the ^{14}C production time series point to a broad removal of this bias.

The preserved cosmogenic radionuclide production variations allowed us to synchronize the $^{10}Be/^{9}Be$-ratios from WGB and KKJ sediments, as well as the $^{10}Be_{TOC}$ record from KKJ sediments to the ^{14}C production time series via curve fitting and reduce the centennial chronological uncertainties to about ±20 (WGB) and ±40 (KKJ) years. Integrating synchronized proxy records from both archives enabled us to interpret a relatively short period of homogenous sediment deposition and ventilation in the central Baltic Sea basins from 6250 to 6000 a BP as possibly triggered by a coinciding mean annual and winter cooling allowing deep water formation during the generally warmer HTM. Such robust multi-archive investigations of short climate events would not have been possible based on the originally centennial-scale uncertainties of the ^{14}C dated sediment records. Future studies with longer ^{10}Be time series could further improve the robustness of the combined Baltic Sea and KKJ sediment chronologies and test our paleoclimate implications.

Acknowledgements

We thank two anonymous reviewers and the editor for their valuable comments. We are grateful to Brian Brademann (GFZ) and Hendrick Mück (IOW) for their help during the coring campaign at Lake Kälksjön, as well as Anne Köhler and Alma Schulz (IOW) for lab assistance. ^{10}Be and ^{9}Be data measured in this study will be published in the PANGAEA data library. Holocene ^{14}C production rates inferred from the IntCal20 calibration curve will be made available upon request by RM.

Author contributions

Markus Czymzik: Designed the study; led the extraction of ^{10}Be from sediment samples; performed the statistical analyses and wrote the initial draft.
Marcus Christl: Conducted ^{10}Be measurements. Contributed to the interpretation of the data and the writing of the final manuscript.
Olaf Dellwig: Performed ^{9}Be measurements. Contributed to the interpretation of the data and the writing of the final manuscript.
Raimund Muscheler: Contributed to the interpretation of the data and the writing of the final manuscript.
Daniela Müller: Contributed to the interpretation of the data and the writing of the final manuscript.
Jérôme Kaiser: Contributed to the interpretation of the data and the writing of the final manuscript.
Markus J Schwab: Contributed to the interpretation of the data and the writing of the final manuscript.
Carla KM Nantke: Contributed to the interpretation of the data and the writing of the final manuscript.
Achim Brauer: Contributed to the interpretation of the data and the writing of the final manuscript.
Helge W Arz: Led XRF and LOI measurements. Contributed to the interpretation of the data and the writing of the final manuscript.

Funding

The author(s) disclosed receipt of the following financial support for the research, authorship, and/or publication of this article: M.Cz. is financed through grants CZ 227/4-1 (SyncBalt project) and CZ 227/7-1 (BaltChron project) of the German Science Foundation (DFG). This publication is a contribution to the BaltRap project SAW-2017-IOW-2, funded by the Leibniz Association.

ORCID iDs

Markus Czymzik https://orcid.org/0000-0003-1599-7643
Marcus Christl https://orcid.org/0000-0002-3131-6652
Jérôme Kaiser https://orcid.org/0000-0002-0290-9088

References

Adolphi F and Muscheler R (2016) Synchronizing the Greenland ice core and radiocarbon timescales over the Holocene – Bayesian wiggle-matching of cosmogenic radionuclide records. *Climate of the Past* 12: 15–30.

Aldahan A and Possnert G (1998) A high-resolution ^{10}Be profile from deep sea sediment covering the last 70ka: Indication for globally synchronized environmental events. *Quaternary Geochronology* 17: 1023–1032.

Andrén E, Andrén T and Kunzendorf H (2000) Holocene history of the Baltic Sea as a background for assessing records of human impact in the sediments of the Gotland Basin. *Holocene* 10: 687–702.

BACC (2015) *Second Assessment of Climate Change for the Baltic Sea Basin*. Heidelberg: Springer.

Balco G, DeJong BD, Ridge JC et al. (2021) Atmospherically produced beryllium-10 in annually laminated late-glacial sediments of the North American Varve Chronology. *Geochronology* 3: 1–33.

Berggren AM, Aldahan A, Possnert G et al. (2010) ^{10}Be and solar activity cycles in varved lake sediments, AD 1900–2006. *Journal of Paleolimnology* 44: 559–569.

Berglund BE, Sandgren P, Barnekow L et al. (2005) Early Holocene history of the Baltic Sea, as reflected in coastal sediments in Blekinge, southeastern Sweden. *Quaternary International* 130: 111–139.

Björck S (1995) A review of the history of the Baltic Sea, 13.0-8.0 ka BP. *Quaternary International* 27: 19–40.

Blockley SPE, Bourne AJ, Brauer A et al. (2014) Tephrochronology and the extended intimate (integration of ice-core, marine and terrestrial records) event stratigraphy 8–128 ka b2k. *Quaternary Science Reviews* 106: 88–100.

Christl M, Vockenhuber C, Kubik PW et al. (2013) The ETH Zurich AMS facilities: Performance parameters and reference materials. *Nuclear Instruments & Methods in Physics Research Section B, Beam Interactions With Materials and Atoms* 294: 29–38.

Croudace I, Löwemark L, Tjallingii R et al. (2019) Current perspectives on the capabilities of high resolution XRF core scanners. *Quaternary International* 514: 5–15.

Czymzik M, Adolphi F, Muscheler R et al. (2016) A varved lake sediment record of the ^{10}Be solar activity proxy for the Lateglacial-Holocene transition. *Quaternary Science Reviews* 153: 31–39.

Czymzik M, Muscheler R, Adolphi F et al. (2018) Synchronizing ^{10}Be in two varved lake sediment records to IntCal13 ^{14}C during three grand solar minima. *Climate of the Past* 14: 687–696.

Czymzik M, Muscheler R, Brauer A et al. (2015) Solar cycles and depositional processes in annual ^{10}Be from two varved lake sediment records. *Earth and Planetary Science Letters* 428: 44–51.

Czymzik M, Nowaczyk NR, Dellwig O et al. (2020) Lagged atmospheric circulation response in the Black Sea region to Greenland interstadial 10. *Proceedings of the National Academy of Sciences of the United States of America* 117: 28649–28654.

Czymzik M, Tjallingii R, Plessen B et al. (2023) Mid-Holocene reinforcement of North Atlantic atmospheric circulation variability from a western Baltic lake sediment record. *Climate of the Past* 19: 233–248.

Dellwig O, Wegwerth A, Schnetger B et al. (2019) Dissimilar behaviors of the geochemical twins W and Mo in hypoxic-euxinic marine basins. *Earth-Science Reviews* 193: 1–23.

Ebisuzaki W (1997) A method to estimate the statistical significance of a correlation when the data are serially correlated. *Journal of Climate* 10: 2147–2153.

Ekman M (1996) A consistent map of the postglacial uplift of Fennoscandia. *Terra Nova* 8: 158–165.

Emeis KC, Struck U, Blanz T et al. (2003) Salinity changes in the central Baltic Sea (NW Europe) over the last 10000 years. *Holocene* 13: 411–421.

Fleitmann D, Cheng H, Badertscher S et al. (2009) Timing and climatic impact of Greenland interstadials recorded in stalagmites from northern Turkey. *Geophysical Research Letters* 36: L19707.

Grant KM, Rohling EJ, Bar-Matthews M et al. (2012) Rapid coupling between ice volume and polar temperature over the past 150,000 years. *Nature* 491: 744–747.

Häusler K, Moros M, Wacker L et al. (2017) Mid- to late Holocene environmental separation of the northern and central Baltic Sea basins in response to differential land uplift. *Boreas* 46: 111–128.

Heaton TJ, Blaauw M, Blackwell PG et al. (2020) The IntCal20 approach to radiocarbon calibration curve construction: A new methodology using Bayesian splines and errors-in-variables. *Radiocarbon* 62: 821–863.

Henken-Mellies WU, Beer J, Heller F et al. (1990) ^{10}Be and ^{9}Be in South Atlantic DSDP Site 519: Relation to geomagnetic reversals and to sediment composition. *Earth and Planetary Science Letters* 98: 267–276.

Jokinen SA, Virtasalo JJ, Jilbert T et al. (2018) A 1500-year multiproxy record of coastal hypoxia from the northern Baltic Sea indicates unprecedented deoxygenation over the 20th century. *Biogeosciences* 15: 3975–4001.

Kaiser J, Tomczak M, Dellwig O et al. (2024) Mediterranean-like "fall dump" events in the Baltic Sea. *Holocene* 34: 415–419.

Kaiser J, van der Meer MTJ and Arz HW (2017) Long-chain alkenones in Baltic Sea surface sediments: New insights. *Organic Geochemistry* 112: 93–104.

Lal D and Peters B (1967) Cosmic ray produced radioactivity on the Earth. In: Flügge S (ed.) *Handbuch Der Physik*. Berlin: Springer, pp.551–612.

Lane CS, Brauer A, Martín-Puertas C et al. (2015) The Late Quaternary tephrostratigraphy of annually laminated sediments from Meerfelder Maar, Germany. *Quaternary Science Reviews* 122: 192–206.

Lecavalier BS, Fisher DA, Milne GA et al. (2017) High Arctic Holocene temperature record from the Agassiz ice cap and Greenland ice sheet evolution. *Proceedings of the National Academy of Sciences of the United States of America* 114: 5952–5957.

Leppäranta M and Myrberg K (2009) *Physical Oceanography of the Baltic Sea*. Berlin, Heidelberg: Springer.

Lisiecki LE and Lisiecki PA (2002) Application of dynamic programming to the correlation of paleoclimate records. *Paleoceanography* 17: 1049.

Meier HEM (2005) Modeling the age of Baltic seawater masses: Quantification and steady state sensitivity experiments. *Journal of Geophysical Research Oceans* 110: C02006.

Mekhaldi F, Czymzik M, Adolphi F et al. (2020) Radionuclide wiggle matching reveals a nonsynchronous early Holocene climate oscillation in Greenland and western Europe around a grand solar minimum. *Climate of the Past* 16: 1145–1157.

Mellström A, Nilsson A, Stanton T et al. (2015) Post-depositional remanent magnetization lock-in depth in precisely dated varved sediments assessed by archaeomagnetic field models. *Earth and Planetary Science Letters* 410: 186–196.

Moros M, Kotilainen AT, Snowball I et al. (2020) Is 'deep-water formation' in the Baltic Sea a key to understanding seabed dynamics and ventilation changes over the past 7,000 years? *Quaternary International* 550: 55–65.

Muscheler R, Adolphi F and Knudsen MF (2014) Assessing the differences between the IntCal and Greenland ice-core time scales for the last 14,000 years via the common cosmogenic radionuclide variations. *Quaternary Science Reviews* 106: 81–87.

Muscheler R, Beer J, Kubik PW et al. (2005) Geomagnetic field intensity during the last 60,000 years based on ^{10}Be and ^{36}Cl from the summit ice cores and ^{14}C. *Quaternary Science Reviews* 24: 1849–1860.

Muscheler R and Heikkilä U (2011) Constraints on long-term changes in solar activity from the range of variability of cosmogenic radionuclide records. *Astrophysics and Space Sciences Transactions* 7: 355–364.

Raisbeck GM, Yiou F, Fruneau M et al. (1981) Cosmogenic ^{10}Be/^{7}Be as a probe of atmospheric transport processes. *Geophysical Research Letters* 8: 1015–1018.

Rasmussen SO, Bigler M, Blockley SP et al. (2014) A stratigraphic framework for abrupt climatic changes during the last glacial period based on three synchronized Greenland ice-core records: Refining and extending the INTIMATE event stratigraphy. *Quaternary Science Reviews* 106: 14–28.

Reimer PJ, Austin WEN, Bard E et al. (2020) The IntCal20 Northern Hemisphere radiocarbon age calibration curve (0–55 cal kBP). *Radiocarbon* 62: 725–757.

Savranskaia T, Egli R, Valet J-P et al. (2021) Disentangling magnetic and environmental signatures of sedimentary ^{10}Be/^{9}Be records. *Quaternary Science Reviews* 257: 106809.

Siegenthaler U (1983) Uptake of excess CO_2 by an outcrop-diffusion model of the ocean. *Journal of Geophysical Research* 88: 3599–3608.

Simon Q, Thouveny N, Bourlès DL et al. (2016) Authigenic ^{10}Be/^{9}Be ratios and ^{10}Be-fluxes (230Thxs-normalized) in central Baffin Bay sediments during the last glacial cycle: Paleoenvironmental implications. *Quaternary Science Reviews* 140: 142–162.

Simon Q, Thouveny N, Bourlès DL et al. (2020) Cosmogenic ^{10}Be production records reveal dynamics of geomagnetic dipole moment (GDM) over the Laschamp excursion (20–60 ka). *Earth and Planetary Science Letters* 550: 116547.

Snowball I, Muscheler R, Zillén L et al. (2010) Radiocarbon wiggle matching of Swedish lake varves reveals asynchronous climate changes around the 8.2 kyr cold event. *Boreas* 39: 720–733.

Stanton T, Snowball I, Zillén L et al. (2010) Validating a Swedish varve chronology using radiocarbon, palaeomagnetic secular variation, lead pollution history and statistical correlation. *Quaternary Geochronology* 5: 611–624.

von Grafenstein U, Erlenkeuser H, Brauer A et al. (1999) A Mid-European decadal isotope-climate record from 15,500 to 5000 years B.P. *Science* 284: 1654–1657.

Wanner H, Solomina O, Grosjean M et al. (2011) Structure and origin of Holocene cold events. *Quaternary Science Reviews* 30: 3109–3123.

Warden L, Moros M, Neumann T et al. (2017) Climate induced human demographic and cultural change in northern Europe during the mid-Holocene. *Scientific Reports* 7: 15251.

Winterhalter B (1992) Late-Quaternary stratigraphy of Baltic Sea basins - a review. *Bulletin - Geological Society of Finland* 64: 189–194.

Wittenborn AK, Radtke H, Dutheil C et al. (2022) A downcore calibration of the TEX_{86}^{L} te mperature proxy for the Baltic Sea. *Continental Shelf Research* 251: 104875.

Wittmann H, von Blanckenburg F, Bouchez J et al. (2012) The dependence of meteoric ^{10}Be concentrations on particle size in Amazon river bed sediment and the extraction of reactive ^{10}Be/^{9}Be ratios. *Chemical Geology* 318-319: 126–138.

Wulf S, Ott F, Słowiński M et al. (2013) Tracing the Laacher See tephra in the varved sediment record of the Trzechowskie palaeolake in central northern Poland. *Quaternary Science Reviews* 76: 129–139.

Ziegler M, Jilbert T, de Lange GJ et al. (2008) Bromine counts from XRF scanning as an estimate of the marine organic carbon content of sediment cores. *Geochemistry Geophysics Geosystems* 9: Q05009.

Zillén L, Conley DJ, Andrén T et al. (2008) Past occurrences of hypoxia in the Baltic Sea and the role of climate variability, environmental change and human impact. *Earth-Science Reviews* 91: 77–92.